Inorganic Chemistry

pubs.acs.org/IC

Article

Unveiling the Stability and Kinetic Pathway from Plutonium Clusters to Colloidal PuO_2 Nanoparticles

Maëva Munoz, Christelle Tamain,* Matthieu Virot, Simon Bayle, Sandrine Dourdain, Thomas Dumas, Pier Lorenzo Solari, Denis Menut, Valérie Vallet, and Dominique Guillaumont

Cite This: *Inorg. Chem.* 2026, 65, 7741−7750

Read Online

ACCESS | Metrics & More | Article Recommendations | Supporting Information

ABSTRACT: The solution stability of plutonium(IV) oxo-hydroxo clusters is a central issue in actinide chemistry, with broad implications for fundamental coordination chemistry, the nuclear fuel cycle, and environmental migration. In this work, we investigate the long-term evolution of the hexanuclear $[Pu_6O_4(OH)_4]^{12+}$ cluster stabilized by acetate ligands. Using ultraviolet−visible (UV−vis) absorption spectroscopy coupled with X-ray absorption (XAS) and small-angle X-ray scattering (SAXS) synchrotron techniques, we probed its structural transformation over nearly one year of aging. UV−vis and XAS analyses revealed a progressive loss of the molecular cluster signature accompanied by the emergence of low Pu−Pu coordination environments (CN = 5−6), characteristic of PuO_2 colloidal nanoparticles. In contrast, SAXS measurements indicated a gradual increase in the apparent particle diameter of up to 10−15 nm, which is inconsistent with the formation of compact 2−3 nm PuO_2 nanoparticles usually observed in aqueous solutions. The combined results most probably support a mechanism in which the hexameric cluster first converts into PuO_2 primary colloids, which subsequently assemble into larger aggregates without crystallographic coalescence.

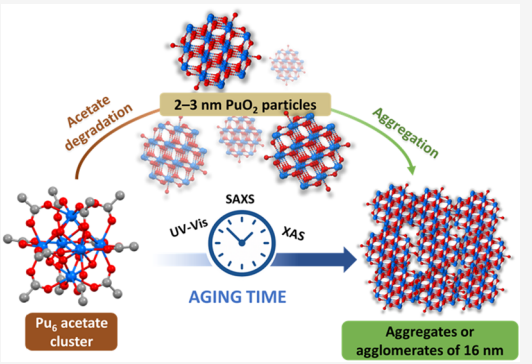

INTRODUCTION

The aqueous chemistry of actinides in near-neutral conditions is strongly influenced by hydrolysis reactions and the formation of well-defined polynuclear structures. Recent studies have highlighted the importance of such entities across diverse domains, including the environmental migration of radionuclides,[1,2] nuclear fuel cycle operations (material balance, separation, waste management···)[3−5] and even biological systems.[6] Despite their relevance, these nanostructures are generally not considered in conventional speciation diagrams, although their formation and stability have been demonstrated across wide pH values and concentration ranges.[5,7−9] Actinide clusters are distinct polynuclear species composed of multiple metal centers bridged by oxo and/or hydroxo groups. Their core structures are characterized by their nuclearity (N), which refers to the number of actinide atoms within the compound. These distinct structures are formed in aqueous media through hydrolysis and condensation reactions (olation and oxolation) and are stabilized at their surface by organic or inorganic ligands.[7] Such stabilization inhibits further condensation into larger particles identified as PuO_2 colloidal nanoparticles or precipitates.[7,8,10−12]

A broad variety of tetravalent actinide clusters have been structurally identified in solution or at the solid state, with N ranging from 2 up to 38.[5,7,8,10,13−30] For plutonium, however, structural data remain comparatively scarce. To date, only three dimeric plutonium structures (N = 2) have been reported: two featuring μ_2−OH bridging groups stabilized by sulfate[31] or nitrate[15] ligands, and one with a μ_2-O bridge stabilized by nitrate ligands.[13] The largest plutonium cluster identified so far is the Pu_{38} species, $[Pu_{38}O_{56}Cl_{54}(H_2O)_8]^{14-}$, stabilized in an inorganic medium by chloride ligands.[14,32,33] Among the known plutonium clusters, the hexanuclear $[Pu_6O_4(OH)_4]^{12+}$ has been the most frequently reported motif.[5,6,8,10,17] This structure (N = 6) is typically stabilized by carboxylate ligands, such as acetate,[8] glycine[17] or DOTA (1,4,7,10-tetraazacyclododecane-1,4,7,10-tetraacetic acid).[10]

In 2020, Sigmon and Hixon extended the known family of Pu clusters by identifying Pu_{16} and Pu_{22} species.[14] These two structures showed nested structural relationships with Pu_{38}, suggesting that nanocluster growth may proceed via the assembly of smaller hexameric building units.

In a recent study, Cot-Auriol et al.[34] identified a ultraviolet−visible near infrared (UV−Vis−NIR) absorption signature consistent with the plutonium hexamer during the spontaneous

Received: December 18, 2025
Revised: March 17, 2026
Accepted: March 24, 2026
Published: April 1, 2026

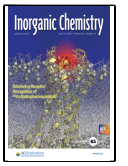

hydrolytic formation of PuO_2 nanoparticles in near-neutral aqueous solutions. In addition, through the observation of a kinetic isotope effect, they demonstrated that both olation and oxolation processes contribute to PuO_2 nanoparticle formation, suggesting that the oxo-hydroxo hexanuclear cluster acts as an intermediate in the colloid formation pathway. In a subsequent study, similar spectroscopic features were observed when carboxylate ligands were introduced into a hydrolyzing solution of Pu(IV).[35] The presence of ligands inhibits the formation of PuO_2, and combined with UV−VIS, extended X-ray absorption fine structure (EXAFS) and SAXS analyses confirmed the hexameric nature of the cluster. While these studies firmly established the spectroscopic signature and recurring occurrence of the hexameric Pu(IV) cluster, its long-term stability remains largely unaddressed, despite its significance for both industrial and environmental contexts. A fundamental question persists: are Pu(IV) oxo-hydroxo clusters thermodynamically stable species, or merely metastable intermediates maintained by kinetic barriers?

In previous work, it was demonstrated that the hexanuclear $[Pu_6O_4(OH)_4]^{12+}$ cluster could be selectively isolated and stabilized by acetate ligands under specific hydrolysis conditions.[8] Its molecular structure was further confirmed in the solution by EXAFS analyses and density functional theory (DFT) models, showing full consistency with the solid-state core. This system therefore provides a relevant and well-characterized model to assess the stability of the hexameric Pu(IV) cluster. In this study, we address this question by investigating the long-term stability and transformation of the acetate-stabilized hexanuclear Pu(IV) cluster, $[Pu_6O_4(OH)_4(AcO)_{12}(H_2O)_6]$. Its structural evolution and potential conversion into PuO_2 colloidal nanoparticles were monitored over nearly one year using UV−Vis absorption spectroscopy with spectral deconvolution and complementary synchrotron-based X-ray scattering (SAXS) and absorption (XAS) techniques.

RESULTS AND DISCUSSION

The reference absorption spectrum of the hexanuclear acetate cluster in the aqueous solution is shown in Figure S1(SI). This spectrum exhibits characteristic absorption bands at 455, 513, 553, 656, 691, and 788 nm, in agreement with previously reported spectra of the acetate-stabilized $[Pu_6O_4(OH)_4]^{12+}$ hexamer.[6,8,10,20] The absorption spectrum of the freshly prepared solution is presented in Figure 1, together with its spectral deconvolution. This analysis indicates that the hexanuclear cluster is the predominant species in solution (91%), with only minor residual contributions. A distinct residual band centered at 478 nm corresponds well to the 470−490 nm features reported by Paramonova et al. for monomeric Pu(IV)−acetate species: $Pu(AcO)^{3+}$, $Pu(AcO)_2^{2+}$, $Pu(AcO)_3^{+}$, and $Pu(AcO)_4$.[36−38] Although the assignment of $Pu(AcO)_4$ to this region is likely a misattribution and instead corresponds to the hexameric cluster $Pu_6O_4(OH)_4(AcO)_{12}(H_2O)_6$,[8] Paramonova's work remains a valuable reference for early monomeric species with 1:1 or 1:2 stoichiometry, supporting the coexistence of monomeric Pu(IV)−acetates with the hexamer in solution.

To follow the effect of time, the initial cluster solution was placed in a plastic tube sealed with a snap cap and stored in the glovebox at ambient temperature and pressure. The spectroscopic signature of the solution was then monitored at regular aging times. Figure 2a compares the absorption spectrum of

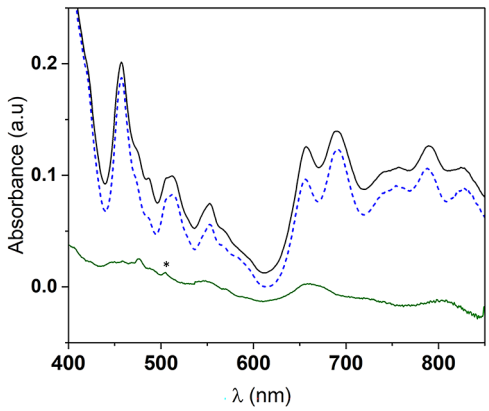

Figure 1. UV−Vis absorption spectrum of Pu(IV)-acetate solution (black), fitted contribution of the $[Pu_6O_4(OH)_4]^{12+}$ cluster (blue dashed, 91%), and residual spectrum (green) showing a monomeric Pu(IV)-acetate band at 478 nm; the Am(III) band from Pu decay is marked with an asterisk.

the initial solution (0 w) with those recorded after 10, 17, 30, and 45 weeks (referred to 10w, 17w, 30w and 45w sample names). The spectra evolved markedly over the studied period, showing a progressive decrease of the 455 nm absorption band from the hexameric cluster upon aging.[6,8,10,20,34,35] Quantitative analyses (Table 1) supported this observation, showing that the fraction of the cluster decreased from 91% in the fresh solution to 68% after 10 weeks, 51% after 17 weeks, 31% after 30 weeks, and finally below 17% after 45 weeks. Complete UV−Vis spectral deconvolutions supporting these trends are provided in the Supporting Information (Figure S2, SI). This behavior clearly demonstrates the gradual loss of stability of the Pu(IV) hexanuclear cluster in solution over time (note that we did not observe the precipitation of any solid phase during this study). Spectral subtraction further revealed the emergence of a residual component whose absorption spectrum resembled that of intrinsic Pu(IV) colloids. Such colloids are known to consist of suspended PuO_2 nanoparticles with diameters of approximately 2−3 nm and exhibit characteristic absorption bands at 508, 578, 614, 687, and 736 nm, along with strong absorption in the near-UV region arising from Mie scattering.[12,39−41] To illustrate this comparison, Figure 2b overlays the residual spectrum obtained after subtraction of the hexameric cluster contribution with a representative absorption spectrum of PuO_2 colloids (Figure S1, Supporting Information). The good correspondence at 508, 578, 687, and 736 nm supports the assignment of the residual signature to PuO_2 colloid species. However, minor discrepancies are observed, particularly around 614 nm and in the near-UV region. Similar discrepancies have already been reported for PuO_2 colloids obtained from various synthetic routes.[12,35] These variations may arise from differences in particle size and shape or from ligand coordination at the particle surface, which may be associated with modifications of the electronic structure. To test this hypothesis, the UV−vis absorption spectrum of aged PuO_2 colloidal nanoparticles, prepared by controlled hydrolysis,[12,39] was recorded before and after the addition of 1 M acetate ligands. Figure 2b shows that the addition of acetate results in an instantaneous modification of the colloidal spectral signature similar to the residual spectrum shown in Figure 2b, (without precipitation) marked by the emergence of new absorption bands at 609 and 636 nm. While the crystalline PuO_2 core of the nanoparticle is

https://doi.org/10.1021/acs.inorgchem.5c05921
Inorg. Chem. 2026, 65, 7741−7750

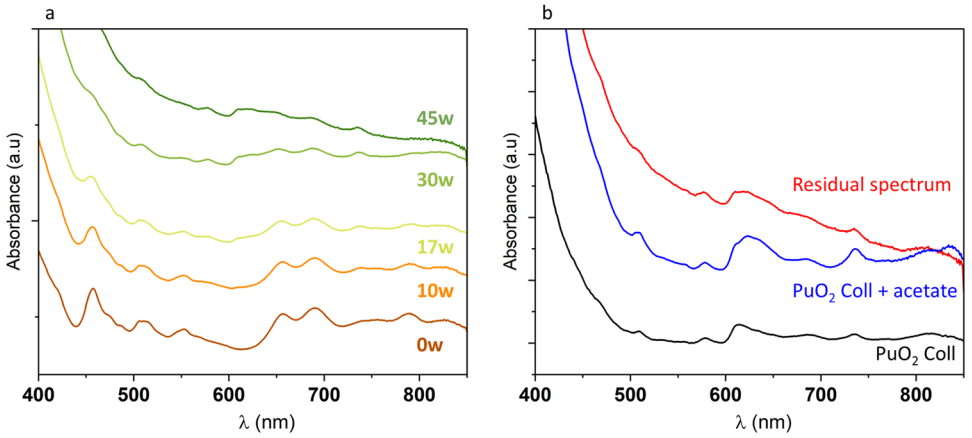

Figure 2. (a) UV−Vis absorption spectra of the hexanuclear Pu(IV)−acetate cluster solution recorded at different aging times: freshly prepared (0 w), 10 weeks (10 w), 17 weeks (17 w), 30 weeks (30 w), and 45 weeks (45 w). (b) Comparison between the residual absorption spectrum obtained after subtraction of the hexameric contribution (red) and PuO_2 colloidal nanoparticles before (black) and after (blue) acetate addition (see Figure S1, SI).

Table 1. Relative Contributions of Pu(IV) Species Obtained from Vis−NIR Spectral Deconvolution and EXAFS LCF Monte Carlo Analyses at Different Aging Times[a]

samples	Pu species (%)			
	$[Pu_6(OH)_4O_4]^{12+}$		Pu(IV) colloid	
	UV−Vis abs.	EXAFS	UV−Vis abs.	EXAFS
0w	91	98 ± 0.08	-	0.2 ± 0.06
10w	68	80 ± 0.10	-	21 ± 0.09
17w	51	49 ± 0.10	-	48 ± 0.08
30w	31	18 ± 0.10	-	82 ± 0.09
45w	17	21 ± 0.10	-	80 ± 0.09

[a]EXAFS uncertainties are reported as 2σ from Monte Carlo resampling.

expected to remain largely unaffected by ligand binding, the nanoparticle surface is likely to be sensitive to changes in its local environment.

The different solutions sampled at 0, 10, 17, 30, and 45 weeks of aging were characterized by EXAFS spectroscopy. XANES analyses confirmed the strong predominance of Pu(IV) in all solutions, as indicated by the characteristic edge position and white line intensity (Figure S3, SI). The corresponding Fourier Transforms (FT) of Pu L_3-edge EXAFS spectra gathered in Figure 3 capture the progressive structural evolution of the polynuclear species from the initial to the final solutions (0w and 45w). The FT from the freshly prepared solution (0w) exhibits well-defined contributions characteristic of an ordered molecular environment, consistent with the structural model of the oxo-hydroxo hexamer $[Pu_6O_4(OH)_4(AcO)_{12}(H_2O)_6]$ reported by Chupin et al.[8] Best-fit EXAFS analysis required five distinct coordination shells. The first shell corresponds to short Pu−μ_3-O^{2-} interactions at 2.20 ± 0.01 Å (CN = 2). A second oxygen shell at 2.39 ± 0.01 Å (CN = 7) accounts for longer Pu−μ_3−OH^-/acetate/H_2O bonds corresponding to mixed coordination by hydroxo groups, acetates, and water molecules, in good agreement with previously reported distances in the range 2.36−2.43 Å.[9,10] A third shell arises from Pu−C scattering contributions of acetate ligands coordinated to the cluster, located at 3.38 ± 0.02 Å (CN = 4). In addition, two Pu−Pu coordination shells are observed at 3.78 ± 0.01 Å (CN = 4) and 5.27 ± 0.03 Å (CN = 1), respectively. These distances are in line with the crystallographic values reported for the hexameric clusters, including those decorated by DOTA ligands.[10,17] The longer Pu−Pu contribution reflects opposite vertices of the octahedral core.[8] Altogether, these EXAFS contributions unambiguously confirm the presence of the

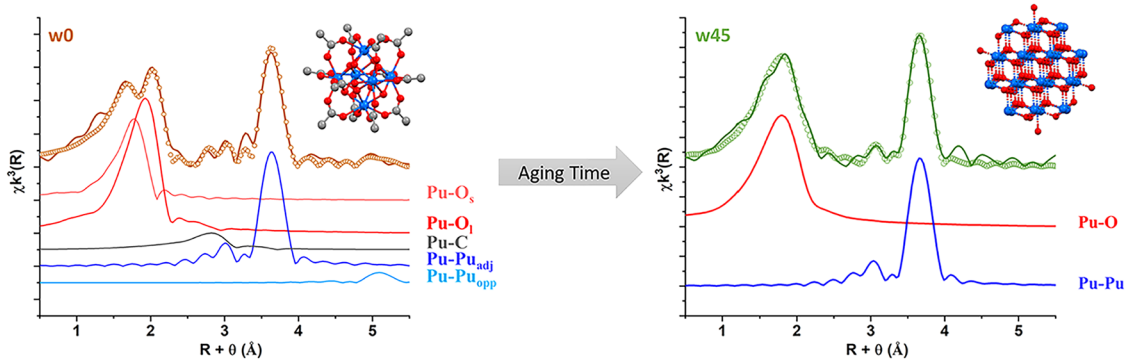

Figure 3. Fourier-Transform of Pu L_3-edge EXAFS spectra between 0 and 5.5 $Å^{-1}$ for the Pu(IV) acetate solutions (0w) and the aged solution (45w). Both FT are characteristic of the hexameric cluster and the PuO_2 colloid, respectively. Experimental data (colored lines) and best-fit results (dashed lines) are obtained using the structural model of the Pu(IV) oxo-hydroxo acetate hexamer or PuO_2. The individual contributions included in the fits are shown below each spectrum.

https://doi.org/10.1021/acs.inorgchem.5c05921
Inorg. Chem. 2026, 65, 7741−7750

hexameric cluster of Pu in the initial solution, in full agreement with the UV−vis spectroscopic observations discussed above.

By contrast, the final solution sampled after 45 weeks of aging shows a markedly different EXAFS spectrum. As shown in Figure 3, the FT reveals a collapse of the first coordination shell into a single Pu−O contribution centered at 2.32 ± 0.01 Å with a coordination number of 8.5 ± 0.7.[12,39] This contribution is accompanied by broadened envelopes, indicative of a more heterogeneous and disordered oxygen environment. The second coordination shell displays a Pu−Pu contribution at 3.81 ± 0.01 Å with CN = 5.4 ± 0.5. Both coordination shells are characteristic of hydrolytic colloids, which have been described as PuO_2 nanoparticles covered by disordered surface oxygens.[12,39] The corresponding EXAFS fitting parameters are reported in Table S1 (SI), together with literature data for the hexameric cluster[8] and PuO_2 colloids.[12] The EXAFS fits for all analyzed solutions are presented in the Supporting Information (Figure S4, SI). Notably, the Pu−O shell exhibits an average distance of 2.32 ± 0.01 Å and a large Debye−Waller factor, reflecting substantial structural disorder related to the presence of multiple types of oxygen atoms, associated with defects or to different environments between core and surface plutonium atoms. These parameters are consistent with the formation of nanosized PuO_2 particles. Overall, these EXAFS observations corroborate the UV−Vis absorption results discussed above and confirm the transformation of the hexanuclear cluster into PuO_2 colloidal nanoparticles upon long-term aging.

To quantify the intermediate structures aged after 10 weeks (10w), 17 weeks (17w), and 30 weeks (30w) of aging, Monte Carlo linear-combination fits (LCF) of the FT EXAFS spectra were performed using the 0 w (hexamer) and the 45w (predominantly colloid) solutions as end members, since they represent well-identified structural fingerprints of the hexamer and of the colloidal state, respectively. It should be noted, however, that the 45w spectrum still contains a residual contribution of the hexamer (approximately 21%), and therefore corresponds to a weighted mixture of clusters and colloids rather than a pure colloidal spectrum. As shown in Figure 4, the EXAFS spectra of the intermediate samples are well reproduced by linear combinations of these two references, indicating that no additional species are required to describe the data. The signature of the hexamer fraction is found to progressively decrease with time, while the one of the colloids increases. These trends are in excellent agreement with the UV−Vis results, demonstrating strong consistency between the two independent techniques. Table 1 compares the quantitative results obtained from both techniques and also reports the relative contributions of each component extracted from the Monte Carlo linear-combination fits for all samples. Uncertainties were estimated by Monte Carlo resampling and are reported as 2σ confidence intervals. Further details, including an example of the χ^2 distribution, are provided in Figure S5 (Supporting Information).[43]

Finally, to isolate the colloidal fraction, the EXAFS spectrum of the 0w hexameric solution was subtracted from the aged data sets (10w, 17w, 30w, and 45w), and the resulting residuals were fitted independently. In these fits, only the amplitude reduction factor (S_0^2) was fixed to 1, while ΔE, R, CN, and σ^2 were allowed to vary. The extracted structural parameters are summarized in Table 2. For the first coordination shell (Pu−O), the large Debye−Waller factors ($\sigma^2 \approx 0.014$−0.019 Å^2) indicate substantial structural disorder related to the presence

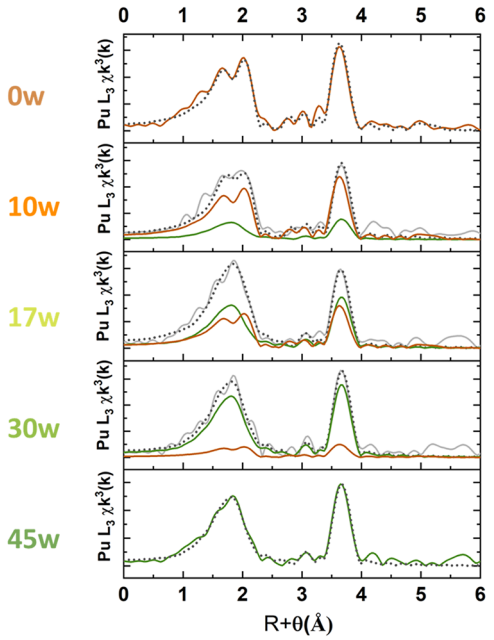

Figure 4. Stacked Fourier transforms (FT) of the Pu L_3-edge EXAFS spectra acquired in the 3.7−16 Å^{-1} range for the 0w, 10w, 17w, 30w, and 45w samples. The 0w and 45w spectra were used as reference end points for the Monte Carlo linear-combination fits (LCF), which were applied to the intermediate 10w, 17w, and 30w samples to illustrate the progressive decrease of the cluster contribution and the concomitant increase of the colloid component. Experimental data are shown as solid lines, best-fit results as dashed lines. The green and brown traces correspond to the colloid and cluster references, respectively.

of multiple types of oxygen atoms, associated with defects or to different environments between core and surface plutonium atoms. Because of the strong correlation between CN and S_0^2 and the residual noise introduced by the spectral subtraction at early aging times, the Pu−O coordination numbers were not considered reliable. Consequently, the analysis focuses on the Pu−O distances and σ^2 values reported in Table 2, which provide robust evidence for a disordered nanoscale oxygen environment.

The Pu−Pu distance remains essentially constant at 3.82 Å across all samples (except for 17w), in good agreement with values reported for hydrolytic PuO_2 colloids.[12,39] By contrast, the Pu−Pu CN increases progressively with aging time. This may reflect the gradual development of a PuO_2 structural backbone.

Taken together, this EXAFS analysis of the colloidal components upon aging samples seems to reveal a subtle and progressive structural evolution toward PuO_2 colloids. Characterized by under-coordinated Pu−O environments and incomplete Pu−Pu shells, this may reflect the formation of gradually more crystalline PuO_2 nanoparticles. However, because EXAFS probes only the short-range atomic structure, it cannot provide direct information on higher-order structural features such as particle size, aggregation stage, or morphology.

To complement the local structure information obtained from EXAFS, Small-Angle X-ray Scattering (SAXS) experiments were performed using synchrotron radiation to probe the morphology and size evolution of the nanoparticles. The freshly prepared cluster sample (0 w) did not exhibit any reliable scattering signal as the sample was polluted by a

https://doi.org/10.1021/acs.inorgchem.5c05921
Inorg. Chem. 2026, 65, 7741−7750

Table 2. Structural Parameters Obtained from the Fits of the EXAFS Data[a]

sample	paths	CN		σ^2 (Å)		R (Å)		ΔE_0 (eV)	χ_{red}^2
10w	Pu−O	13.9	±2.7	0.019	±0.003	2.34	±0.08	−1.73	20.18
	Pu−Pu	3.0	±1.8	0.006	±0.003	3.82			
17w	Pu−O	9.2	±1.5	0.013	±0.002	2.35	±0.06	−1.3	12.9
	Pu−Pu	4.5	±0.7	0.007	±0.001	3.80			
30w	Pu−O	8.9	±0.1	0.014	±0.001	2.34	±0.02	−0.9	4.27
	Pu−Pu	5.9	±0.9	0.007	±0.001	3.82			
45w	Pu−O	8.3	±0.7	0.014	±0.001	2.34	±0.08	−1.1	4.30
	Pu−Pu	5.8	±0.7	0.01	±0.001	3.82			

[a]The fits were based on the structural parameters of colloidal PuO2 nanoparticles after subtraction of the $[Pu_6O_4(OH)_4]^{12+}$ cluster contribution. S_0^2 = 1. R-factor <3%

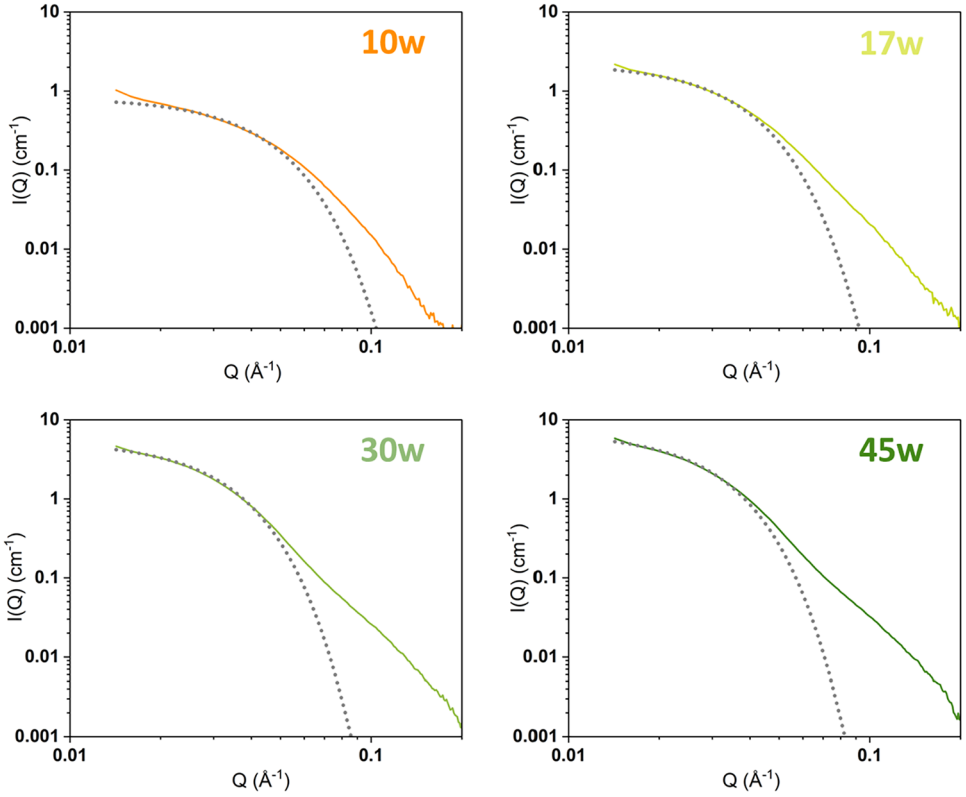

Figure 5. Small-angle X-ray scattering (SAXS) profiles (colored lines) and corresponding Guinier model fits (dashed lines) applied on the Pu(IV) solutions 10w, 17w, 30w and 45w.

precipitate that was formed under the beam. This behavior contrasts with previous SAXS studies devoted to the characterization of $[Pu_6O_4(OH)_4]^{12+}$ clusters stabilized with various ligands where the plutonium concentration was lower (0.5 mM compared to 4 mM in the present work).[35,42] Nevertheless, the scattered signal in this work was also very noisy evidencing the instrumental sensitivity limits for such very diluted systems. Nevertheless, previous SAXS investigations of the oxo-hydroxo hexamer $[Pu_6O_4(OH)_4]^{12+}$ stabilized by acetate ligands reported a characteristic radius of approximately 0.6 nm,[35] which is therefore taken as a reference for the initial molecular cluster size. The SAXS curves in the Q range of 0.01−0.1 $Å^{-1}$ obtained for the aged samples (10 w to 45 w) are shown in Figure 5. The full Q range and superimposed data are presented in the Supporting Information section (Figure S6). In all cases, the scattering intensity reaches a plateau at low Q and decreases in Q^{-4} at high Q values. This behavior is consistent with previous reports on PuO_2 colloids, although the inflection between these two regimes is shifted to lower Q-values, indicating the presence of larger objects.[12] From 0 to 45 weeks, the progressive shift of the inflection toward lower Q values, together with the marked increase in scattering intensity, indicates the formation of larger objects over time. Although aggregation decreases the number of individual scattering entities in solution, the strong size dependence of the SAXS intensity results in an overall increase of the scattering signal as the average object size grows.

A Guinier analysis was employed to obtain a first approximation of the radius of the scattering objects. For diluted solutions with minimal particle interactions, eq 1 can be used to fit the low-Q region and the inflection of the curves in order to extract a radius of gyration R_g (valid for $QR_g < 1$). R_g is highly sensitive to the particle size and shape. Assuming solid and spherical particles, eq 2 was subsequently used to determine the corresponding particle radius.

https://doi.org/10.1021/acs.inorgchem.5c05921
Inorg. Chem. 2026, 65, 7741−7750

Table 3. Particle Radius Obtained from SAXS Data for Samples w10, w17, w30 and w45[a]

Fit	radius (nm)			
Fit (SAS View)	10w	17w	30w	45w
Guinier approach	6.0 ± 3.0	6.8 ± 1.0	7.7 ± 0.5	8.1 ± 0.7
monodispersed sphere form factor	5.7 ± 1.1	6.2 ± 1.3	7.2 ± 0.3	7.4 ± 0.6
monodispersed sphere form + polydispersity (0.4)	3.7 ± 1.9	4.2 ± 1.0	4.8 ± 0.6	5.0 ± 0.5
2 sphere form factors including one for a cluster with parameters from Dumas et al.[42] and Cot-Auriol et al.[35]	5.8 ± 1.1	6.1 ± 1.3	7.2 ± 0.7	7.7 ± 0.6
Similar as above with polydispersity (0.4) for the unknown sphere and 0.2 for the cluster[42]	3.7 ± 1.9	4.1 ± 1.0	4.8 ± 0.6	5.0 ± 0.5

[a]A progressive increase of the nanoparticle size is observed with the cluster solution aging.

$$I(Q) = I_0 \exp(-(QR_G)^2/3) \quad (1)$$

$$R_G = R\sqrt{(3/5)} \quad (2)$$

where, I_0 is the initial intensity at very small angles (Q approaching 0 value), R_g is the radius of gyration, and R is the radius of the spherical particle.

The radii obtained from this analysis are gathered in Table 3 and show a progressive increase with aging time, from 6.0 nm (10w) to 6.8 nm (17w), 7.7 nm (30w) and 8.1 nm (45w). Additional approaches were tested to improve the fit quality, particularly at high Q-values. Fits achieved using a monodisperse sphere form factor (Figure S7 (SI)) gave radii consistent with those obtained from the Guinier analysis and confirm the presence of objects larger than 10 nm in diameter. Although the monodisperse model reasonably reproduces the overall signal, the absence of oscillations in the experimental curves indicates substantial polydispersity. Introducing a size polydispersity of approximately 40% suppresses the oscillations in the simulated curves but still results in noticeable deviations from the experimental data at high Q (Figure S8, SI). These discrepancies likely arise from the coexistence of additional smaller polynuclear species in solution, including small colloids or residual polynuclear clusters. We have finally tested a fractal model. While particle sizes obtained could have been adapted to our system, the fit yielded nonphysical values for the fractal dimension. At this stage, the reported results represent a compromise between the experimental observations and the constraints imposed by earlier literature. Additional complexity in the fitting models would require strong assumptions, and further investigations. Nevertheless, these results clearly highlight the impact of aging time and of the presence of organic ligands on the structural properties of the colloids, and show that all extracted particle sizes remain substantially higher than those previously reported for PuO_2 nanoparticles (2−3 nm).[11,12,40,42,44]

To place our results in context, we compared them with previous investigations of PuO_2 colloidal nanoparticles. Several studies have focused on the local structure of PuO_2 nanoparticles formed in aqueous solution using different approaches (hydrolysis, sonochemistry, ammonia addition, etc.) and have demonstrated, from L_3-edge EXAFS spectra, a broadening of the Pu−O shell (associated with a large DWF) together with a decrease in the Pu−Pu coordination number as particle size decreases, while maintaining Pu−O and Pu−Pu distances characteristic of the fluorite PuO_2 structure. This behavior has been attributed to the nanoparticle size effect, where surface moieties (under-coordinated species, hydroxylated groups, defects, and bond length distribution) contribute to a decrease in the apparent Pu−Pu coordination numbers and modification of the O-shell due to their large probed proportion relative to the bulk one.

First, UV−vis absorption spectroscopy unequivocally showed the signature of PuO_2 colloidal nanoparticles. Second, EXAFS analyses of all aged solutions consistently yielded local structures compatible with PuO_2, with Pu−Pu coordination numbers below 5.9. While demonstrating the formation of PuO_2 colloidal nanoparticles by hydrolysis in pure water, previous studies reported coordination numbers of CN= 5.0−5.7 for the Pu−Pu shell for 2−3 nm PuO_2 nanoparticles (HR-TEM and SAXS).[11,12] Similarly, PuO_2 nanoparticles prepared via ammonia addition in Pu aqueous solutions showed Pu−Pu coordination number of 3.2−4.5 for particle sizes between 1.6 and 3.2 nm, as determined by HR-TEM and XRD.[40] These Pu−Pu CN values strongly differ from the bulk PuO_2 theoretical one (CN= 12) and are consistent with nanoscale particles in the 2−3 nm size range. The strong agreement between our data and those from earlier studies suggests that, despite different experimental conditions (acetate medium, nitrate systems, ammonia, etc.), common structural features have emerged that are best explained by the formation of 2−3 nm PuO_2 primary nanoparticles. These nanoparticles are generally described as having a crystalline fluorite-type PuO_2 core surrounded by a structurally disordered Pu−Pu under-coordinated surface layer (incomplete Pu−Pu shells).[12,33,39,45,46]

In contrast, SAXS analysis of the acetate-containing solutions systematically indicates the presence of much larger scattering objects, exceeding 10 nm in diameter after 45 weeks of aging. When considered alongside the local structural information from EXAFS results, these sizes raise important questions: compact PuO_2 nanoparticles larger than 10 nm would be expected to exhibit Pu−Pu coordination numbers in the 10−12 range according to the apparent CN value proposed by Romanchuk formula,[47] which is not observed.[12,47] This apparent inconsistency strongly suggests that the entities detected by SAXS are not compact PuO_2 nanoparticles. A more plausible interpretation is that the SAXS signal arises from loose assemblies of 2−3 nm PuO_2 primary nanoparticles, whose under-coordinated surface environments remain consistent with previous studies. Altogether, our results support a mechanism in which 2−3 nm primary colloids form at early aging stages and progressively assemble into larger aggregates without crystallographic coalescence. In this framework, EXAFS probes the local coordination within individual subunits, whereas SAXS is sensitive to their aggregation and spatial organization. To conclude, the system is most likely a nanoparticle polydispersity coupled with an additional presence of small oligomeric and cluster species, as evidenced by SAXS fit models.

Such behavior is reminiscent of observations, for instance, reported by Bots et al., who studied the formation of U(VI) clarkeite-type colloids under geologically relevant pH conditions.[48] In that study, the colloids were shown to consist of

https://doi.org/10.1021/acs.inorgchem.5c05921
Inorg. Chem. 2026, 65, 7741−7750

1.5−1.8 nm primary nanoparticles that partially assembled into 20−60 nm aggregates that remained stable for more than 2.5 years. Combined with our findings, this suggests that the aging of plutonium hexameric clusters in the presence of organic ligands leads to previously unrecognized nanoscale effects with the formation of nanoparticle aggregates (nanoparticles of 2−3 nm). The hexamers evolve to form nanoparticles of 2−3 nm, that are probably complexed on the surface by the remaining acetate ligands as suggested by the UV−vis spectra presented in Figure 2b. The specific role of the acetate ligands in these aggregates remains unclear as they can either create bridges between nanoparticles and actively take part to the aggregation process, or just affect the chemical environment around the nanoparticles allowing their association and the formation of 16 nm aggregates. Additional investigations are currently underway to further elucidate these ligand-induced effects.

CONCLUSIONS

In this study, we examined the solution stability and temporal evolution of Pu(IV) acetate-stabilized hexameric clusters. Our results demonstrate that these molecular entities are not indefinitely stable in aqueous solutions but, instead, undergo a gradual transformation into PuO_2 colloidal nanoparticles. EXAFS analyses reveal the persistence of low Pu−Pu coordination environments, characteristic of small, under-coordinated (Pu−Pu contributions) species and consistent with previously reported hydrolytic PuO_2 colloids. In contrast, SAXS measurements indicate a steady increase in the apparent particle size, reaching values significantly larger than those typically reported for compact 2−3 nm PuO_2 nanoparticles. At first glance, this trend appears inconsistent with the EXAFS-derived local structure, which remains characteristic of nanoscale PuO_2. Taken together, these complementary observations support a transformation mechanism in which the hexanuclear Pu(IV) clusters first convert into 2−3 nm PuO_2 colloids that subsequently associate into larger aggregates rather than forming compact crystalline domains directly. A key question to emerge from these results is whether this evolution reflects the intrinsic thermodynamic instability of hexameric clusters, making them transient. As this process occurs with aging, the question of acetate degradation in solution in this process remains open. In particular, the role of radiolysis in degrading organic molecules needs to be investigated. Disentangling these contributions represents an important perspective for future work and will be essential for a deeper understanding of actinide cluster and colloid formation mechanisms. Additionally, the interrelation between particle size and local structure in regards of surface complexation by ligands seems also questioned by our results. This point will be addressed in further investigations.

EXPERIMENTAL SECTION

Caution! The element plutonium is a strongly radioactive α-emitter, and it is a highly toxic heavy metal. The element was manipulated inside gloveboxes within ATALANTE (Marcoule, France) nuclear facility under strict radiological control.

Reagents

The used isotopic mixture was mainly composed of ^{239}Pu (75%), which has a half-life of $t_{1/2}(^{239}Pu)$ = 24,110 years. The initial plutonium solution (0.6 M) was stabilized at the tetravalent state in nitric acid medium (1.2 M). Glacial acetic acid and solid $LiOH.H_2O$ were purchased by Fisher Scientific. Concentrated nitric acid (68%) was provided by VWR Chemicals. The pH of the solutions was measured using a Metrohm pH electrode calibrated against standard buffers.

Synthesis of $Pu_6O_4(OH)_4(CH_3COO)_{12}$ Cluster

The preparation of $[Pu_6O_4(OH)_4(CH_3COO)_{12}]$ cluster in aqueous solution was performed following the procedure described by Chupin et al.[8] Five milliliters of an aqueous ligand-acetate solution were prepared by mixing 573 μL of glacial acetic acid and 277 mg of $LiOH.H_2O$ (0.66 mol·L^{-1} Li^+) in deionized water to form a 10 mL solution with $[AcOH]_{tot}$ = 1 M and pH = 4.5. Then, 30 μL of Pu(IV) nitric stock solution was diluted in 4.97 mL of the above-described solution to reach a final plutonium concentration of 3.9 mM.

UV−Vis−NIR Absorption Spectroscopy

UV−Vis−NIR absorption spectra were recorded using a Cary 5000 spectrophotometer (Agilent Technologies) operated inside glove-boxes. Spectra were collected from 350 to 900 nm plastic cuvettes with an optical path length of 1 cm. For each spectrum, a baseline correction was performed using the corresponding blank solution previously prepared by replacing the Pu volume with an equivalent volume of 1.2 mol·L^{-1} HNO_3 in the acetate solution.

Synchrotron Measurements

Small-Angle X-ray Scattering (SAXS) and X-ray Absorption Spectroscopy (XAS) measurements were performed on the MARS beamline at the SOLEIL Synchrotron Radiation Facility (Saint-Aubin, France; 2.75 GeV, 500 mA). The beamline is equipped with a double-crystal monochromator (DCM) framed by two mirrors for beam collimation and rejection of higher-order harmonics. Five plutonium samples were aliquoted at defined time points (0, 10, 17, 30, and 45 weeks) and labeled according to their aging time as 0w, 10w, 17w, 30w, and 45w, respectively. For each defined aging time (0, 10, 17, 30, and 45 weeks), aliquots were sampled and immediately characterized by UV−Vis spectroscopy. The solutions were then frozen for storage prior to synchrotron measurements. Before SAXS and XAS experiments at the SOLEIL facility, the samples were defrosted and an additional UV−Vis measurement was performed to check that no significant evolution or loss of the hexamer contribution occurred during storage. No detectable changes were observed. Each solution was sampled and transferred into double layered Teflon sample cells (250 μL capacity), sealed with Kapton films to ensure double radiological containment.

Small-Angle X-ray Scattering (SAXS). SAXS data were collected at an X-ray energy of 17 keV using a Pilatus 2 M CdTe detector (Dectris AG, Switzerland) positioned764 mm from the sample. Energy calibration was performed using the yttrium K-edge (17,038 eV). Suppression of higher-order harmonics and vertical beam focusing were achieved through the use of the Pt-coated stripes on the mirrors placed before and after the Si(220) double-crystal monochromator (DCM, 3.1 mrad). A beam stop was positioned in front of the detector and placed within a helium-filled chamber to reduce air scattering. Angular calibration was conducted using the known diffraction pattern of silver behenate. Scattering intensity profiles, I(Q), were obtained by azimuthally integrating the isotropic 2D scattering patterns using the pyFAI software. The resulting absolute intensity was corrected for acquisition time, sample transmission, and thickness, and scaled using a calibration constant derived from a reference polyethylene sample ($I(Q)$ = 4.9 cm^{-1} at Q = 0.36 nm^{-1}). The final scattering intensity from the solutions was given after subtraction of the cell and solvent contributions.

Pu L_3 Edge XAS. XAS spectra were recorded in fluorescence mode at the Pu L_3-edge (E_0 = 18,057 eV) using an X-PIPS 13-element Si detector (MIRION Technologies SAS, France). The sample holder was oriented at 45° with respect to the incident X-ray beam. Energy calibration was performed using a Zr metal foil at the K-edge defined at 17,998 eV. Each spectrum represents the average of three consecutive scans. XANES analysis confirmed the presence of mainly Pu(IV) in all solutions, as indicated by the characteristic edge position and white line intensity (Figure S9, SI). EXAFS data were processed with Athena and Artemis software (IFEFFIT package).[49] After pre-edge subtraction and spline background removal, normalization and

https://doi.org/10.1021/acs.inorgchem.5c05921
Inorg. Chem. 2026, 65, 7741−7750

k^3-weighting were applied on the data. Fourier transforms (FT) were performed on the EXAFS oscillation between 3.7 and 16 $Å^{-1}$, using a Kaiser-Bessel window. Fitting was performed in R-space, using a structural model derived from the Pu(IV) oxo-hydroxo acetate hexamer defined previously, and including five scattering paths (μ_3-O^{2-}, μ_3–OH, C, Pu_{adj} and Pu_{opp}).[8] Coordination numbers (CN), interatomic distances (R), and Debye–Waller factors (σ^2) were considered as floating parameters, while S_0^2 was fixed to 1.

Monte Carlo Estimation of EXAFS LCF Contributions and Uncertainties (2σ)

Monte Carlo resampling was applied to the linear combination fits (LCF) to determine both the relative fractions of Pu(IV) present as hexametric clusters or colloids and their associated uncertainties. This method provides statistically robust confidence intervals by exploring the full-parameter space and accounting for correlations between fitting parameters.[43] For each intermediate sample obtained after 10w, 17w and 30w, the LCF approach was performed using 0w (initial cluster) and 45w (aged solution converted into colloids) as reference spectra, with two free weights (w_1 and w_2). The procedure involved (i) the generation of a large number of random weight distributions (typically 10^4–10^5 trials), (ii) the calculation of a χ^2 for each trial with the plot of the difference $\chi^2 - \chi_{min}^2$ as a function of the weights. The optimal contributions corresponded to the weight values at χ_{min}^2 and are reported in Table 1.

The variance was calculated with the following equation (eq 3)

$$S^2 = \frac{\min(\chi^2)}{N - p} \tag{3}$$

where, N is the number of data points (approximately 240 for k = 3.7–16 $Å^{-1}$) and p the number of free parameters (p = 2 for w_1 and w_2). The 2σ confidence interval was defined as $6.18*s^2$ (two free parameters). The intersections between the $\chi^2 - \chi^2$min envelope and this threshold gave the lower and upper bounds of the 2σ confidence interval. An example of this procedure is given in Figure S4 (SI) for the sample 17w.

■ ASSOCIATED CONTENT

Supporting Information

The Supporting Information is available free of charge at https://pubs.acs.org/doi/10.1021/acs.inorgchem.5c05921.

Additional results and interpretations including vis–NIR spectroscopy, EXAFS, and SAXS data (PDF)

■ AUTHOR INFORMATION

Corresponding Author

Christelle Tamain – *CEA, DES, ISEC, DMRC, Univ Montpellier, Marcoule 30207, France;* orcid.org/0000-0002-3492-6536; Email: christelle.tamain@cea.fr

Authors

Maëva Munoz – *CEA, DES, ISEC, DMRC, Univ Montpellier, Marcoule 30207, France;* orcid.org/0009-0002-3101-0917

Matthieu Virot – *ICSM, Univ Montpellier, CEA, CNRS, ENSCM, Marcoule 30207, France;* orcid.org/0000-0002-6295-2555

Simon Bayle – *CEA, DES, ISEC, DMRC, Univ Montpellier, Marcoule 30207, France;* orcid.org/0000-0003-3851-5459

Sandrine Dourdain – *ICSM, Univ Montpellier, CEA, CNRS, ENSCM, Marcoule 30207, France;* orcid.org/0000-0003-4828-4092

Thomas Dumas – *CEA, DES, ISEC, DMRC, Univ Montpellier, Marcoule 30207, France;* orcid.org/0000-0001-6425-6484

Pier Lorenzo Solari – *Synchrotron SOLEIL, L'Orme des Merisiers, Saint-Aubin 91190, France*

Denis Menut – *Synchrotron SOLEIL, L'Orme des Merisiers, Saint-Aubin 91190, France;* orcid.org/0000-0001-8657-3333

Valérie Vallet – *Université de Lille, CNRS, UMR 8523—PhLAM-Physique des Lasers Atomes et Molécules, F-59000 Lille, France;* orcid.org/0000-0002-2202-3858

Dominique Guillaumont – *CEA, DES, ISEC, DMRC, Univ Montpellier, Marcoule 30207, France;* orcid.org/0000-0002-9329-5623

Complete contact information is available at: https://pubs.acs.org/10.1021/acs.inorgchem.5c05921

Notes

The authors declare no competing financial interest.

■ ACKNOWLEDGMENTS

V.V. acknowledges support from the French Ministry of Higher Education and Research, the Hauts de France Regional Council, and the European Regional Development Fund (ERDF) through the CPER WaveTech@HdF project. The authors thank Elise Guerinoni for her assistance with the SAXS analyses. The authors also wish to thank the CEA for its support and funding, as well as the RCHIM project of the RTA program for its support. V.V. acknowledges the French State under the France-2030 program and the Initiative of Excellence of the University of Lille for funding and support provided to the R-CDP-24-003-AREA project. Additional support from the French Ministry of Higher Education and Research, the Hauts-de-France Regional Council, and the European Regional Development Fund (ERDF) through the project WaveTech@HdF is also acknowledged.

■ REFERENCES

(1) Kersting, A. B. Plutonium Transport in the Environment. *Inorg. Chem.* **2013**, *52* (7), 3533–3546.

(2) Marsac, R.; Banik, N. L.; Marquardt, C. M.; Kratz, J. V. Stabilization of Polynuclear Plutonium(IV) Species by Humic Acid. *Geochim. Cosmochim. Acta* **2014**, *131*, 290–300.

(3) Neck, V.; Kim, J. I. Solubility and Hydrolysis of Tetravalent Actinides. *Radiochim. Acta* **2001**, *89* (1), 1–16.

(4) Vanagas, N. A.; Wacker, J. N.; Rom, C. L.; Glass, E. N.; Colliard, I.; Qiao, Y.; Bertke, J. A.; Van Keuren, E.; Schelter, E. J.; Nyman, M.; Knope, K. E. Solution and Solid State Structural Chemistry of Th(IV) and U(IV) 4-Hydroxybenzoates. *Inorg. Chem.* **2018**, *57* (12), 7259–7269.

(5) Tamain, C.; Dumas, T.; Hennig, C.; Guilbaud, P. Coordination of Tetravalent Actinides (An = Th^{IV}, U^{IV}, Np^{IV}, Pu^{IV}) with DOTA: From Dimers to Hexamers. *Chem. – Eur. J.* **2017**, *23* (28), 6864–6875.

(6) Daronnat, L.; Holfeltz, V.; Boubals, N.; Dumas, T.; Guilbaud, P.; Martinez, D. M.; Moisy, P.; Sauge-Merle, S.; Lemaire, D.; Solari, P. L.; Berthon, L.; Berthomieu, C. Investigation of the Plutonium(IV) Interactions with Two Variants of the EF-Hand Ca-Binding Site I of Calmodulin. *Inorg. Chem.* **2023**, *62* (21), 8334–8346.

(7) Knope, K. E.; Soderholm, L. Solution and Solid-State Structural Chemistry of Actinide Hydrates and Their Hydrolysis and Condensation Products. *Chem. Rev.* **2013**, *113* (2), 944–994.

(8) Chupin, G.; Tamain, C.; Dumas, T.; Solari, P. L.; Moisy, P.; Guillaumont, D. Characterization of a Hexanuclear Plutonium(IV)

Nanostructure in an Acetate Solution via Visible−Near Infrared Absorption Spectroscopy, Extended X-Ray Absorption Fine Structure Spectroscopy, and Density Functional Theory. *Inorg. Chem.* **2022**, *61* (12), 4806−4817.
(9) Takao, K.; Takao, S.; Scheinost, A. C.; Bernhard, G.; Hennig, C. Formation of Soluble Hexanuclear Neptunium(IV) Nanoclusters in Aqueous Solution: Growth Termination of Actinide(IV) Hydrous Oxides by Carboxylates. *Inorg. Chem.* **2012**, *51* (3), 1336−1344.
(10) Tamain, C.; Dumas, T.; Guillaumont, D.; Hennig, C.; Guilbaud, P. First Evidence of a Water-Soluble Plutonium(IV) Hexanuclear Cluster. *Eur. J. Inorg. Chem.* **2016**, *2016* (22), 3536−3540.
(11) Dalodière, E.; Virot, M.; Dumas, T.; Guillaumont, D.; Illy, M.-C.; Berthon, C.; Guerin, L.; Rossberg, A.; Venault, L.; Moisy, P.; Nikitenko, S. I. Structural and Magnetic Susceptibility Characterization of Pu(V) Aqua Ion Using Sonochemistry as a Facile Synthesis Method. *Inorg. Chem. Front.* **2018**, *5* (1), 100−111.
(12) Micheau, C.; Virot, M.; Dourdain, S.; Dumas, T.; Menut, D.; Solari, P. L.; Venault, L.; Diat, O.; Moisy, P.; Nikitenko, S. I. Relevance of Formation Conditions to the Size, Morphology and Local Structure of Intrinsic Plutonium Colloids. *Environ. Sci. Nano* **2020**, *7* (8), 2252−2266.
(13) Ray, D.; Xie, J.; White, J.; Sigmon, G. E.; Gagliardi, L.; Hixon, A. E. Experimental and Quantum Mechanical Characterization of an Oxygen-Bridged Plutonium(IV) Dimer. *Chem. − Eur. J.* **2020**, *26* (36), 8115−8120.
(14) Sigmon, G. E.; Hixon, A. E. Extension of the Plutonium Oxide Nanocluster Family to Include $\{Pu_{16}\}$ and $\{Pu_{22}\}$. *Chem. − Eur. J.* **2019**, *25* (10), 2463−2466.
(15) Knope, K. E.; Skanthakumar, S.; Soderholm, L. Two Dihydroxo-Bridged Plutonium(IV) Nitrate Dimers and Their Relevance to Trends in Tetravalent Ion Hydrolysis and Condensation. *Inorg. Chem.* **2015**, *54* (21), 10192−10196.
(16) Vanagas, N. A.; Wacker, J. N.; Rom, C. L.; Glass, E. N.; Colliard, I.; Qiao, Y.; Bertke, J. A.; Van Keuren, E.; Schelter, E. J.; Nyman, M.; Knope, K. E. Solution and Solid State Structural Chemistry of Th(IV) and U(IV) 4-hydroxybenzoates. *Inorg. Chem.* **2018**, *57* (12), 7259−7269.
(17) Knope, K. E.; Soderholm, L. Plutonium(IV) Cluster with a Hexanuclear $[Pu_6(OH)_4O_4]^{12+}$ Core. *Inorg. Chem.* **2013**, *52* (12), 6770−6772.
(18) Vanagas, N. A.; Higgins, R. F.; Wacker, J. N.; Asuigui, D. R. C.; Warzecha, E.; Kozimor, S. A.; Stoll, S. L.; Schelter, E. J.; Bertke, J. A.; Knope, K. E. Mononuclear to Polynuclear UIV Structural Units: Effects of Reaction Conditions on U-Furoate Phase Formation. *Chem. − Eur. J.* **2020**, *26* (26), 5872−5886.
(19) Wacker, J. N.; Vasiliu, M.; Colliard, I.; Ayscue, R. L. I.; Han, S. Y.; Bertke, J. A.; Nyman, M.; Dixon, D. A.; Knope, K. E. Monomeric and Trimeric Thorium Chlorides Isolated from Acidic Aqueous Solution. *Inorg. Chem.* **2019**, *58* (16), 10871−10882.
(20) McCusker, T. L.; Vanagas, N. A.; Szymanowski, J. E. S.; Surbella, R. G.; Bertke, J. A.; Arteaga, A.; Knope, K. E. Elucidating Trends in Synthesis and Structural Periodicity in a Series of Tetravalent Actinide−Oxo Hexamers. *CrystEngComm* **2025**, *27* (4), 507−515.
(21) Duval, S.; Béghin, S.; Falaise, C.; Trivelli, X.; Rabu, P.; Loiseau, T. Stabilization of Tetravalent 4f (Ce), 5d (Hf), or 5f (Th, U) Clusters by the $[\alpha\text{-}SiW_9O_{34}]^{10-}$ Polyoxometalate. *Inorg. Chem.* **2015**, *54* (17), 8271−8280.
(22) Travia, N. E.; Scott, B. L.; Kiplinger, J. L. A Rare Tetranuclear Thorium(IV) μ_4-Oxo Cluster and Dinuclear Thorium(IV) Complex Assembled by Carbon−Oxygen Bond Activation of 1,2-Dimethoxyethane (DME). *Chem. − Eur. J.* **2014**, *20* (51), 16846−16852.
(23) Falaise, C.; Volkringer, C.; Loiseau, T. Mixed Formate-Dicarboxylate Coordination Polymers with Tetravalent Uranium: Occurrence of Tetranuclear $\{U_4O_4\}$ and Hexanuclear $\{U_6O_4(OH)_4\}$ Motifs. *Cryst. Growth Des.* **2013**, *13* (7), 3225−3231.
(24) Chatelain, L.; Faizova, R.; Fadaei-Tirani, F.; Pécaut, J.; Mazzanti, M. Structural Snapshots of Cluster Growth from U_6 to U_{38} During the Hydrolysis of UCl_4. *Angew. Chem., Int. Ed.* **2019**, *58* (10), 3021−3026.
(25) Hennig, C.; Takao, S.; Takao, K.; Weiss, S.; Kraus, W.; Emmerling, F.; Scheinost, A. C. Structure and Stability Range of a Hexanuclear Th(IV)−Glycine Complex. *Dalton Trans.* **2012**, *41* (41), 12818−12823.
(26) Falaise, C.; Neal, H. A.; Nyman, M. U(IV) Aqueous Speciation from the Monomer to UO_2 Nanoparticles: Two Levels of Control from Zwitterionic Glycine Ligands. *Inorg. Chem.* **2017**, *56* (11), 6591−6598.
(27) Hu, Y.-J.; Knope, K. E.; Skanthakumar, S.; Soderholm, L. Understanding the Ligand-Directed Assembly of a Hexanuclear Th^{IV} Molecular Cluster in Aqueous Solution. *Eur. J. Inorg. Chem.* **2013**, *2013* (24), 4159−4163.
(28) Woidy, P.; Kraus, F. $[Th_{10}(\mu\text{-}F_{16})(\mu_3\text{-}O_4)(\mu_4\text{-}O_4)(NH_3)_{32}](NO_3)_8{\cdot}19.6\ NH_3$ − the Largest Thorium Complex from Solution Known to Date. *Z. Anorg. Allg. Chem.* **2014**, *640* (8−9), 1547−1550.
(29) Dufaye, M.; Martin, N. P.; Duval, S.; Volkringer, C.; Ikeda-Ohno, A.; Loiseau, T. Time-Controlled Synthesis of the 3D Coordination Polymer $U(1,2,3\text{-}Hbtc)_2$ Followed by the Formation of Molecular Poly-Oxo Cluster $\{U_{14}\}$ Containing Hemimellitate Uranium(IV). *RSC Adv.* **2019**, *9* (40), 22795−22804.
(30) Soderholm, L.; Almond, P. M.; Skanthakumar, S.; Wilson, R. E.; Burns, P. C. The Structure of the Plutonium Oxide Nanocluster $[Pu_{38}O_{56}Cl_{54}(H_2O)_8]^{14-}$. *Angew. Chem., Int. Ed.* **2007**, *47*, 298−302, DOI: 10.1002/anie.200704420.
(31) Wester, D. W. Synthesis and Characterization of Bis(μ-Hydroxo)Tetraaquadiplutonium(IV) Sulfate, $Pu_2(OH)_2(SO_4)_3{\cdot}4H_2O$, a Novel Compound Containing Hydrolyzed Plutonium(IV). *Inorg. Chem.* **1982**, *21* (9), 3382−3385.
(32) Wilson, R. E.; Skanthakumar, S.; Soderholm, L. Separation of Plutonium Oxide Nanoparticles and Colloids. *Angew. Chem., Int. Ed.* **2011**, *50*, 11234−11237, DOI: 10.1002/anie.201105624.
(33) Soderholm, L.; Almond, P. M.; Skanthakumar, S.; Wilson, R. E.; Burns, P. C. The Structure of the Plutonium Oxide Nanocluster $[Pu_{38}O_{56}Cl_{54}(H_2O)_8]^{14}$-. *Angew. Chem., Int. Ed.* **2008**, *47* (2), 298−302.
(34) Cot-Auriol, M.; Virot, M.; Dumas, T.; Diat, O.; Menut, D.; Moisy, P.; Nikitenko, S. I. First Observation of $[Pu_6(OH)_4O_4]^{12+}$ Cluster during the Hydrolytic Formation of PuO2 Nanoparticles Using H/D Kinetic Isotope Effect. *Chem. Commun.* **2022**, *58* (94), 13147−13150.
(35) Cot-Auriol, M.; Dourdain, S.; Dumas, T.; Tamain, C.; Menut, D.; Hunault, M. O. J. Y.; Solari, P. L.; Moisy, P.; Nikitenko, S. I.; Virot, M. Capturing the Elusive: A Snapshot of the Pu(IV) Hexanuclear Cluster Intermediate in the Birth of PuO_2 Colloidal Nanoparticles. *Inorg. Chem.* **2025**, *64* (34), 17178−17188.
(36) Paramonova, V. I.; Dubrovin, V. S. Complexation Reactions Of Tetravalent Plutonium With Acetate Ion 0.2. Ion-exchange Study By The Relative Sorption Method. *Sov. Radiochem.* **1980**, *22* (3), 317−321.
(37) Paramonova, V. I.; Dubrovin, V. S. Complexation Reactions Of Tetravalent Plutonium With Acetate Ion 0.1. Ion-exchange Study By Fronaeus Method. *Sov. Radiochem.* **1980**, *22* (3), 310−317.
(38) Paramonova, V. I.; Dubrovin, V. S. Investigation Of The Complex-formation Reaction Of Quadrivalent Plutonium With Acetate Ion 0.3. Spectrophotometric Reaction Investigation. *Sov. Radiochem.* **1980**, *22* (5), 546−551.
(39) Virot, M.; Dumas, T.; Cot-Auriol, M.; Moisy, P.; Nikitenko, S. I. Synthesis and Multi-Scale Properties of PuO_2 Nanoparticles: Recent Advances and Open Questions. *Nanoscale Adv.* **2022**, *4* (23), 4938−4971.
(40) Gerber, E.; Romanchuk, A. Y.; Weiss, S.; Kuzenkova, A.; Hunault, M. O. J. Y.; Bauters, S.; Egorov, A.; Butorin, S. M.; Kalmykov, S. N.; Kvashnina, K. O. To Form or Not to Form: PuO_2 Nanoparticles at Acidic pH. *Environ. Sci.: Nano* **2022**, *9* (4), 1509−1518.
(41) Gerber, E.; Romanchuk, A. Y.; Pidchenko, I.; Amidani, L.; Rossberg, A.; Hennig, C.; Vaughan, G. B. M.; Trigub, A.; Egorova, T.;

https://doi.org/10.1021/acs.inorgchem.5c05921
Inorg. Chem. 2026, 65, 7741−7750

Bauters, S.; Plakhova, T.; Hunault, M. O. J. Y.; Weiss, S.; Butorin, S. M.; Scheinost, A. C.; Kalmykov, S. N.; Kvashnina, K. O. The Missing Pieces of the PuO_2 Nanoparticle Puzzle. *Nanoscale* **2020**, *12* (35), 18039−18048.
(42) Dumas, T.; Virot, M.; Menut, D.; Tamain, C.; Micheau, C.; Dourdain, S.; Diat, O. Size and Structure of Hexanuclear Plutonium Oxo-Hydroxo Clusters in Aqueous Solution from Synchrotron Analysis. *J. Synchrotron Radiat.* **2022**, *29* (1), 30−36.
(43) Curis, E.; Bénazeth, S. About Estimation of Fitted Parameters' Statistical Uncertainties in EXAFS. Critical Approach on Usual and Monte Carlo Methods. *J. Synchrotron Radiat.* **2005**, *12* (3), 361−373.
(44) Powell, B. A.; Dai, Z.; Zavarin, M.; Zhao, P.; Kersting, A. B. Stabilization of Plutonium Nano-Colloids by Epitaxial Distortion on Mineral Surfaces. *Environ. Sci. Technol.* **2011**, *45* (7), 2698−2703.
(45) Ekberg, C.; Larsson, K.; Skarnemark, G.; Ödegaard-Jensen, A.; Persson, I. The Structure of Plutonium(IV) Oxide as Hydrolysed Clusters in Aqueous Suspensions. *Dalton Trans.* **2013**, *42* (6), 2035−2040.
(46) Martin, P.; Grandjean, S.; Ripert, M.; Freyss, M.; Blanc, P.; Petit, T. Oxidation of Plutonium Dioxide: An X-Ray Absorption Spectroscopy Study. *J. Nucl. Mater.* **2003**, *320* (1), 138−141.
(47) Romanchuk, A.; Trigub, A.; Plakhova, T.; Kuzenkova, A.; Svetogorov, R.; Kvashnina, K.; Kalmykov, S. Effective Coordination Numbers from EXAFS: General Approaches for Lanthanide and Actinide Dioxides. *J. Synchrotron Radiat.* **2022**, *29* (Pt 2), 288−294.
(48) Bots, P.; Morris, K.; Hibberd, R.; Law, G. T. W.; Mosselmans, J. F. W.; Brown, A. P.; Doutch, J.; Smith, A. J.; Shaw, S. Formation of Stable Uranium(VI) Colloidal Nanoparticles in Conditions Relevant to Radioactive Waste Disposal. *Langmuir* **2014**, *30* (48), 14396−14405.
(49) Ravel, B.; Newville, M. ATHENA, ARTEMIS, HEPHAESTUS: Data Analysis for X-Ray Absorption Spectroscopy Using IFEFFIT. *J. Synchrotron Radiat.* **2005**, *12* (4), 537−541.

https://doi.org/10.1021/acs.inorgchem.5c05921
Inorg. Chem. 2026, 65, 7741−7750